ELSEVIER

Journal of Power Sources 85 (2000) 72–78

JOURNAL OF POWER SOURCES

www.elsevier.com/locate/jpowsour

A method for measurement and interpretation of impedance spectra for industrial batteries

Eckhard Karden *, Stephan Buller, Rik W. De Doncker

Institute for Power Electronics and Electrical Drives (ISEA), Aachen University of Technology (RWTH), Jägerstr. 17–19, D-52066 Aachen, Germany

Accepted 22 September 1999

Abstract

Impedance spectroscopy is a promising tool for the modeling and diagnosis of industrial batteries. This paper discusses methodological questions connected with the measurement and interpretation of the impedance of such batteries, especially nonlinearity, voltage drift, stability, reproducibility, half-cell measurements, model structure and parameter extraction with respect to quantities like state of charge (SOC). On the basis of this discussion, a specialized impedance spectroscope for industrial batteries has been developed, as well as modifications of the standard electrochemical impedance spectroscopy (EIS) algorithm. A mini-cycle technique is suggested that gains additional information compared to classical measurements with continuous dc current offset. Impedance spectra from lead/acid batteries for different dc currents, SOCs, and temperatures are presented and analyzed. Reference-electrode measurements allow for separation of the half-cell impedances. Emphasis is placed on the limits of experimental reproducibility due to ''history'' of the battery.

Keywords: Lead/acid battery; Electrochemical impedance spectroscopy (EIS); Dynamical modeling; State of charge; State of health

1. Introduction

The basic experiment of electrochemical impedance spectroscopy (EIS) consists in applying a small, sinusoidal voltage or current signal to an electrochemical cell, measuring the system's response (current or voltage, respectively) with respect to amplitude and phase (or, equivalently, real and imaginary part), determining the impedance of the system by complex division of ac voltage by ac current, and repeating this for a certain range of different frequencies. This frequency-domain analysis requires that the system under investigation (1) is linear or at least can be linearized with respect to signal amplitudes in its working point and (2) is stationary or at least quasistationary for the time of measurement. Interpretation of the results and proper modeling requires (3) that the experimental setup allows some idealization like separating between working electrode and reference electrode or maintaining the concentrations of reactants essentially constant at the interface. During recent decades, this method has often been applied in the investigation of electrode (interface reaction) or transport processes as well as in fields like characterization of materials and corrosion science. Several impedance-measuring devices are now available from manufacturers of electrochemical instrumentation, often as plug-in accessories for potentiostats/galvanostats. Control and measurement of the ac signals is usually done by analog circuits for high frequencies and by digital computation employing digital/analog and analog/digital converters for low frequencies [1].

AC or impedance techniques have been applied to batteries, too. An extensive review of works devoted to lead/acid and nickel/cadmium batteries has recently been published [2]. It turns out that two important problems in battery application technology can be tackled with this methodology: (1) dynamic modeling of battery behavior and (2) diagnosis of quantities like actual capacity, state of charge (SOC) and state of health (SOH). Some ''battery testers'' are commercially available that work on single frequencies, usually so high that essentially the ohmic part of cell impedance is measured. They obtain good reliability in identifying cell failures inside large batteries — especially for those battery types and applications where

* Corresponding author. E-mail: ka@isea.rwth-aachen.de; URL: http://www.isea.rwth-aachen.de/

0378-7753/00/$ - see front matter
PII: S0378-7753(99)00385-7

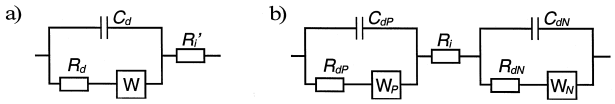

Fig. 1. Basic equivalent circuit of electrochemical half-cells (a) and cells (b) (R_i ohmic resistance, R_d charge-transfer resistances, C_d double-layer capacities, W Warburg impedances).

failure is usually related to a sharp increase of ohmic resistance. Valve-regulated lead/acid batteries (AGM technology) in stand-by applications with permanent float charging may serve as an example [3] where grid corrosion and water loss in the separator are expected to be the dominating aging mechanisms.

A better insight into the truly electrochemical processes, electrode properties, and also transport characteristics, can of course be obtained by extending the frequency range into the millihertz region. However, when applying impedance-measurement techniques to industrial batteries in contrast to usual laboratory cells, a number of additional experimental and theoretical difficulties arise which will be discussed in Section 2. After that, a specially designed EIS instrumentation for industrial batteries is outlined which has been developed and constructed in our laboratory. Modifications of the algorithm for the measurement are suggested, especially for evaluating the influence of dc current bias. Experimental results are presented for 100 Ah Planté lead/acid batteries with respect to reproducibility, dc-current working point, SOC, temperature, differences between individual cells, and half-cell separation using a reference electrode. The experimental findings are interpreted in terms of an equivalent circuit based on the commonly accepted model Fig. 1.

2. Specific requirements for impedance spectroscopy of batteries

Problems that arise when applying the methods of EIS to batteries may be grouped into three categories which will be discussed in detail below. First, batteries are usually operated at currents so large that the *nonlinearity* of transport and reaction processes cannot be neglected. Second, batteries change their structure while being discharged or charged, and they are typically operated until at least one species of reactants depletes (*nonstationarity*). Third, geometry, reaction kinetics and mass transport in large porous electrodes are much more involved and less controllable than in a laboratory cell (*nonideality*); the reaction zone may for example move during discharge from the surface of the plate down the pores, and also from the top part of the plates to the bottom, parasitic reactions like dissociation of electrolyte may occur, and in the case of lead/acid batteries the conducting ions in the electrolyte are also reactants.

These considerations make clear that the scope of possible results is restricted when EIS is performed with batteries as fabricated instead of typical experimental cells. However, impedance spectroscopy provides a unique tool for analysis of the dynamical behavior of batteries. Compared to step–response methods, harmonic small-signal excitation of the system allows for measuring its nonlinearities directly as well as very slow dynamics, and the model parameters obtained are closely related to the underlying physicochemical processes. As a tool for indicating the SOC or SOH which requires only variation and measurement of current and/or voltage it could avoid the need of frequent capacity tests and additional sensors. The following criteria were developed with respect to the use of EIS as a tool for modeling and diagnosis of industrial batteries.

2.1. Requirements resulting from the nonstationarity of battery impedance

- Batteries undergo a structural change when a discharging or charging current flows. A quasistationary description is thus restricted to times small compared to the discharge (or charge) time for a given dc current (measured as ratio to nominal current). This defines a current-dependent lower frequency limit, below which a frequency-domain analysis does not make sense.
- Battery voltage does not define well the state of the battery; in extreme cases the battery may be discharged or charged at exactly the same voltage, depending only on its SOC and history. This suggests that spectroscopy of batteries should always be performed in the galvanostatic mode.
- The equilibrium voltage of the cell (which usually depends on SOC) as well as ''slow'' overvoltages (e.g., in relaxation after a change of current) cause a dc voltage drift while measuring the impedance for each single frequency. Thus a voltage-drift compensation is necessary that requires additional on-line data processing. A generalization of Fourier transform has been suggested for this purpose [4]. Instead, we use a numerical approximation based on the average values of voltage during each period of the exciting sine current.
- Each impedance $Z(\omega)$ measured one after another with a superimposed dc current belongs to a slightly different SOC. Expressing impedance spectra as a function of SOC requires numerical interpolation.
- A battery's behavior and, thus, impedance, is influenced by its ''history'', e.g., via memory effects or inhomogeneous concentration of electrolyte. Spectra from a given battery measured at exactly the same values of (ϑ, I_{dc}, SOC) will show some variation with the former treatment of the battery. Thus, care has to be taken in defining reproducible situations for EIS measurements. The influence of history may partly be introduced into the equivalent-circuit model using initial conditions or feedback. An example is discussed below.

2.2. Requirements resulting from the nonlinearity of battery impedance

- Batteries are typically operated at such currents that linearization of the impedance elements is, in general, not possible. Thus the differential impedance $Z = \mathrm{d}U/\mathrm{d}I$ is not equal to the quotient U/I, and the ac excitation has to be small compared to typical battery currents. The ac current amplitude should be decreased with increasing impedance $|Z|$ such that the voltage-response amplitude does not strongly vary with frequency and never exceeds the linearizable region.
- Analysis of the large-signal behavior is, however, possible by measuring the impedance at several working points defined by dc currents I_{dc} and integrating $U = \int Z(I_{dc})\mathrm{d}I_{dc}$ [5].

2.3. Requirements resulting from the nonideality of battery impedance

- Apart from temperature ϑ and dc current I_{dc}, battery impedance depends on the battery's SOC which is essentially proportional to the integrated current $\int I_{dc}\mathrm{d}t$. Thus, the elements of an equivalent-circuit model of the battery (cf. Fig. 1) are functions of temperature, dc current, and SOC. For a quantitative description, a numerical procedure has to provide parameters for these functions which are simultaneously consistent with a large number of measured impedance spectra $Z(\omega, \vartheta\ I_{dc}$, SOC).
- Battery impedance is usually measured at the terminals of the battery, i.e., as the sum of the electrode (half-cell) impedances. Insertion of reference electrodes is impossible in many practical applications. Apart from that, if mass transport in the electrolyte is significant, the location of a reference electrode becomes critical. However, for laboratory experiments an apparatus is desirable which allows for simultaneous measurement of both half-cell voltages.

3. Experimental

Laboratory instrumentation (called EISmeter in this paper) has been developed at ISEA for high-precision impedance measurements of industrial batteries with nominal voltages up to 12 V. A direct current up to ± 10 A (optionally ± 40 A) is superimposed with the ac excitation. The ac current amplitude may vary from 1 mA to 4 A, depending on the measured impedance. Ac voltage amplitudes are usually chosen to be in the order of 0.3 to 3 mV. These low ac amplitudes allow for linearized analysis of the impedance (small signal) while the battery is being operated at a dc-current working point, far from integral linearity. The frequency range covered by the instrument is 10 kHz to few microhertz. The use of fast digital/analog and analog/digital converters as well as a Pentium PC allow completely digital control and analysis. For measurements in a series connection of up to 14 cells (or half-cells) a new control system is under construction which employs a digital signal processor (DSP). Very high long-term stability of the instrumentation allows for measurements at virtually any low frequency. Theoretical calculations and reference measurements performed with a coaxial resistor (precision shunt, 1 mΩ) show that an impedance of 1 mΩ can be determined in the whole frequency and dc-current range with an error in measurement of less than 2% in amount ($|Z|) = \sqrt{Re^2 Z + Im^2 Z)}$ and less than 2° in phase ($\varphi = \arctan(Im\ Z/Re\ Z)$). Apart from EIS, the device permits arbitrary programming of current patterns with up to 60,000 samples/s [6].

For application of even higher dc currents we have developed a software extension for a commercial battery test-bench (Digatron BTS-600) [7]. Limited only by the current capability of the given test bench, the maximum current is in our case increased to ± 300 A. However, due to the slow sampling rate of this test bench, the upper frequency limit is now shifted to 3 Hz. Apart from that, impedance measurements are performed applying exactly the same algorithm as in the purpose-design EISmeter described above.

Impedance spectroscopy is performed in the galvanostatic mode by superimposing a small alternating current to different direct currents corresponding to practical discharge or charge rates. The ac current amplitude is varied from frequency to frequency iteratively. This guarantees that the ac voltage response remains always in the linear regime. The ac amplitudes were limited to a maximum voltage of 5 mV and a maximum current of 1 A (EISmeter) or 5 A (Digatron), respectively.

The ac current signal is applied at a fixed frequency and amplitude for at least three sine periods and (for frequencies above 0.33 Hz) more than 10 s, always starting and ending with a phase angle of 0. The first sine period is never used for the integration of voltage response in order to allow for a relaxation time in the order of the time constant under investigation. Ideally one would prefer to have several sine periods instead of just one for relaxation, but this would lead to unacceptably long measuring times in the millihertz range. In order to minimize the amplitude of relaxation processes, the frequency is varied in small steps (eight frequencies per decade), starting from the maximum frequency, and the number of sine periods is always integer.

The differential impedance is determined on-line by discrete Fourier transform (DFT). The calculation incorporates a correction for the dc-voltage drift which inevitably will occur if the battery is being discharged or charged during the impedance measurement. The minimum frequency is chosen with respect to the superimposed dc

current such that each sine period is small compared to the discharge (or charge) time.

The cells investigated in this work were 16 Planté-type vented lead/acid batteries (4GroE 100 Ah). After commissioning the cells were cycled several times at 20°C with I_{10} in order to stabilize their capacities. Then the capacities of all cells were investigated as functions of temperature and discharge current by performing discharge/charge cycles at temperatures of 20, 40, and 60°C with different discharge currents between 10 A ($=I_{10}$) and 95 A. Additional experiments were devoted to examination of the current/voltage characteristics in float operation at the three temperatures. That means that each cell was subjected to cycling and floating tests on the Digatron BTS-600 within 4 to 10 weeks, partly at elevated temperatures, and differing in detail from cell to cell. For example, some cells skipped the tests at 40°C, but had more cycles at 20°C with different currents, etc. It turned out that the capacities of the cells were significantly higher than the nominal value (up to 146 Ah at I_{10} and 20°C) but strongly variable from cell to cell. These characterization experiments are beyond the scope of this paper. Possible aging effects due to the cycling tests could not be quantified (though some visible sludging was observed very early, especially at elevated temperatures) and are thus neglected in the discussion of measured impedances.

Impedance spectra were recorded during the characterization experiments mentioned above with two different experimental procedures.

(1) Continuous discharge/charge: Several spectra were measured continuously while the battery was being discharged or charged with a constant dc current. For dc currents from ± 10 to ± 95 A these experiments were performed on the Digatron test-bench during the cycling experiments using our software extension. With dc currents from 0 to ± 10 A we used the EISmeter while the battery was not connected to the Digatron battery test-bench.

(2) Mini-cycles: Starting from rest in a given SOC, the battery is discharged by less than $10\% \cdot K_N$ with a given dc current and then immediately recharged with the same but opposite dc current for the same time. One impedance spectrum is recorded during the discharge period, one during the charge period. Such a mini-cycle is followed by a rest period of at least 1/2 h before the next mini-cycle, usually with another dc current. The mini-cycle experiments were only performed using the EISmeter and limited to SOC $\leq 70\%$ and dc currents up to 10 A. This ensured that charging efficiency was always very close to unity. In fact, additional impedance spectra taken during the rest periods (i.e., with a pure ac current) showed no variation within our limits of accuracy and thus indicated that the battery remained essentially in the same state during a series of three or four mini-cycles.

All impedance measurements reported in the following were made at 20°C unless mentioned otherwise.

4. Results and discussion

4.1. Comparison of continuous discharge/charge vs. mini-cycle technique

Fig. 2 allows a comparison between the two experimental techniques explained above. The first spectrum (dotted line) was recorded in the depth of discharge (DOD) range 30–35% while the battery was being continuously discharged by $-I_{10}$, starting from the fully charged state. At DOD ≈ 35%, we switched from the continuous discharge mode to the mini-cycle mode by recharging the battery with $+I_{10}$ by $5\% \cdot K_N$. Three discharge/charge mini-cycles between DODs 30% and 35% were performed subsequently, always using the same dc current of ± 10 A. The resulting spectra (the last of which is plotted in Fig. 2 as solid line) showed good coincidence with each other (standard deviation $< 2\%$), confirming that the battery impedance does not significantly change from one mini-

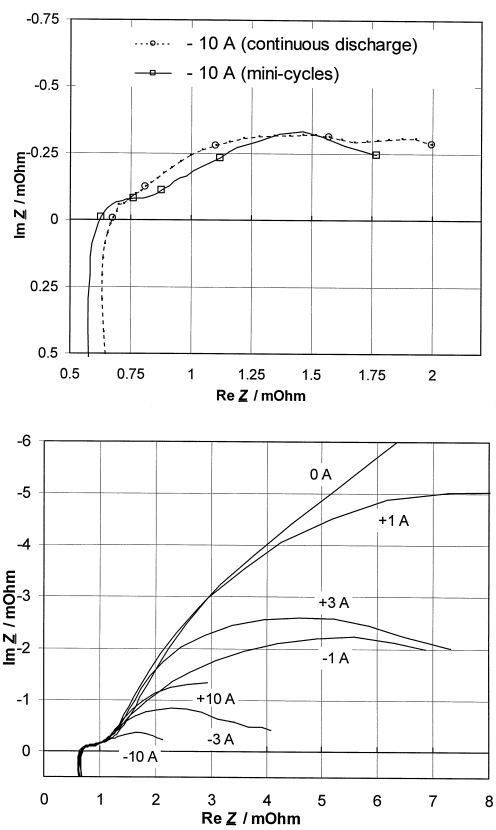

Fig. 2. Impedance plots at depth of discharge (DOD) ≅ 30%, $I_{dc} = -10$ A, $\vartheta = 20$°C, cell no. 14, measured during continuous discharge (dotted line) and in discharge/charge mini-cycles (solid line). The points belonging to frequencies $f = 92$ Hz, 9.2 Hz, 920 mHz, 92 mHz, 9.2 mHz are marked with circles or squares, respectively.

Fig. 3. Impedance plots at DOD ≈ 30% for different dc currents, measured in discharge/charge mini-cycles at $\vartheta = 20$°C at cell no. 14. Minimum frequency: 1 mHz for $|I_{dc}| = 0$–3 A; 7 mHz for $|I_{dc}| = 10$ A (charging currents are counted positive).

cycle to the next. On the other hand, the mini-cycle spectra showed remarkable differences to the spectrum measured during continuous discharge at the same values of (ϑ, I_{dc}, SOC). Please note that in the complex-plane representation of Fig. 2 frequency is hidden as a curve parameter, and that in fact similar impedance values were obtained for frequencies varying by a factor of ten with both methods, respectively.

These differences may be explained by ''nonideality'' effects, e.g., different acid-concentration profiles in both situations and different spatial distribution of the electrochemical reaction within the porous electrodes. Partly, these effects may be included in an equivalent-circuit model of the battery, e.g., by representing electrolyte diffusion during rest periods. However, there will remain certain limits of reproducibility for impedance measurements of batteries. These limits have to be carefully explored especially if impedance measurements are intended to serve as a diagnostic tool. The mini-cycle approach offers an opportunity to partly eliminate the influence of acid diffusion which in the continuous discharge/charge technique tends to obscure the purely electrochemical phenomena.

4.2. Variation of battery impedance with superimposed dc current

Fig. 3 shows complex-plane plots for different superimposed dc currents at almost constant DOD and at constant temperature. They were recorded in the mini-cycle technique described above. When mini-cycles with the same dc current were applied repeatedly, a standard deviation of less than 2% demonstrated good reproducibility of the results. The spectra of Fig. 3 show that the battery is inductive for frequencies $f > 200$ Hz, mainly due to geometry effects. A small semicircle dominates the impedance in a frequency region 200 Hz $> f >$ 5 Hz. It does not show significant variation with current, indicating that the corresponding RC element of the equivalent circuit may be

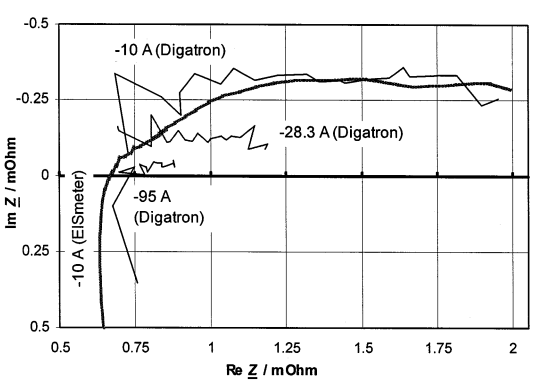

Fig. 4. Impedance plots at DOD ≈ 30% for different dc currents above 10 A, measured during continuous discharge at $\vartheta = 20$°C at cell no. 14. Minimum frequency: 7 mHz for $|I_{dc}| = 10$ A; 13 mHz for $|I_{dc}| = 28.3$ A; 40 mHz for $|I_{dc}| = 95$ A. Maximum frequency (Digatron): 3.33 Hz.

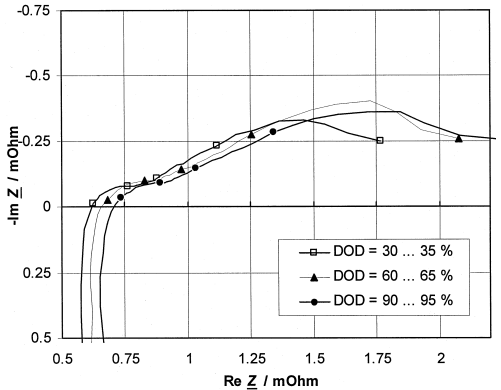

Fig. 5. Impedance plots at $I_{dc} = -10$ A for different DOD, measured in discharge/charge mini-cycles at $\vartheta = 20$°C at cell no. 14. Minimum frequency: 7 mHz. The points corresponding to frequencies $f = 92$ Hz, 9.2 Hz, 920 mHz, 92 mHz, 9.2 mHz are marked.

assumed as linear for these low currents ($I \leq I_{10}$). On the other hand, a strong nonlinearity appears in the low-frequency arcs of the Nyquist plots which obeys a mass-transport (modified Warburg) law in a frequency region 10 Hz $> f >$ 0.1 Hz. The curvature of the Warburg part of the impedance plot for lowest frequencies can be attributed to a boundary condition which is in accordance with earlier measurements [8], [7]. Comparison of the different curves for different currents shows that the $I_{dc} = 0$ curve serves as an asymptote for both discharging and charging currents tending towards zero. Charging impedances are in general larger than the corresponding values for the same, but opposite-sign discharging currents. This reflects the asymmetry of electrode (and transport) kinetics.

Fig. 4 shows impedances measured at higher dc currents measured with the Digatron test-bench in the continuous-discharge mode, compared to a -10 A spectrum recorded with the EISmeter in the same mode. The first four points of each Digatron spectrum with $f > 1$ Hz are obtained with less than 10 samples per period (sampling rate 10 s^{-1}). In addition the voltage resolution of the Digatron test bench (20 V range, 16 Bit: LSB = 300 μV) is much lower than in the EISmeter (10 μV). For the impedances in the order of 1 mΩ these two limitations lead to large errors in measurement, visible as scattering of measured points around a smooth curve. In contrast, the corresponding EISmeter curve also shown in Fig. 2 demonstrates that this is only an effect of the measurement, not of the system. Future measurements of such small impedances with the Digatron will be performed using higher ac signal amplitudes. However, Fig. 4 already indicates the order of magnitude of high-current battery impedance up to the 1-h rate.

4.3. Variation of battery impedance with SOC

Fig. 5 shows how the impedance varies with the battery's SOC or DOD, respectively. Similar to Fig. 3, mini-

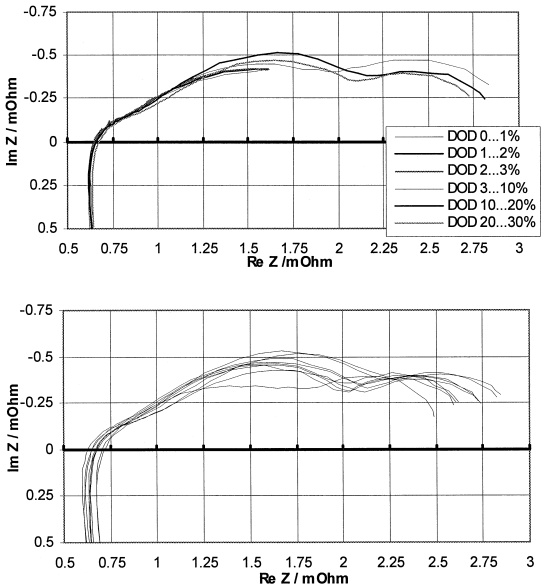

Fig. 6. Impedance plots measured during continuous discharge with $I_{dc} = -10$ A for different DOD, $\vartheta = 20$°C at cell no. 7. Minimum frequency: 280 mHz (short curves: DOD = 0–3%) and 2.8 mHz (long curves: DOD = 3–30%).

Fig. 7. Impedance plots of nine cells (no. 2 to 10) at DOD ≅ 20–30%, $I_{dc} = -10$ A, $\vartheta = 20$°C, measured during continuous discharge. Minimum frequency: 280 mHz.

cycles were applied after the cell had been discharged, starting from 0% DOD, in steps to 30%, 60%, and 90% DOD. From the different dc currents, the −10 A discharge curves were selected for the figure. The 30% curve is again repeated from Fig. 2. Comparison of the three curves shows that mainly the ohmic resistance and the diameter of the low-frequency arc increase with DOD.

Fig. 6 shows similar results which were obtained during continuous discharge in a DOD range 0–30%. The first three spectra were recorded immediately after beginning of discharge only in the high-frequency range, each of the next three spectra was measured in a time corresponding to a 10% change in DOD. At least three arcs can be distinguished in the latter three spectra. The high-frequency part ($f > 3$ Hz) undergoes almost no change during this part of the discharge process. The next part (3 Hz $> f >$ 50 mHz) is a depressed semicircle which grows initially to a maximum and then shrinks again. The low-frequency semicircle ($f < 50$ mHz) shrinks with increasing DOD.

4.4. Variation of impedance from cell to cell

Exactly the same procedure as presented in Fig. 6 was applied to nine of the cells, and the results shows excellent qualitative agreement. For the DOD range 20–30% the nine resulting curves, including the last curve of Fig. 6 for cell no. 7, are shown in Fig. 7. The same impedance spectra are presented in a different way in Fig. 8: The impedance values measured at each cell for some fixed frequencies are plotted against cell number. The cell numbers are sorted by the measured actual capacity which is also inserted in the diagram a dotted line. It turns out that there is some correlation between low-frequency impedance in this DOD range and capacity. The differences between the cells due to manufacturing, temperature and cycling history are too large to allow for a more detailed statistical or physicochemical analysis, but further experiments in this direction seem promising.

4.5. Variation of battery impedance with temperature

Corresponding to Fig. 6, the same procedure was also applied to the same cells at 60°C. Fig. 9 shows the results which are qualitatively the same as for 20°C, but reduced in modulus by approximately one-third.

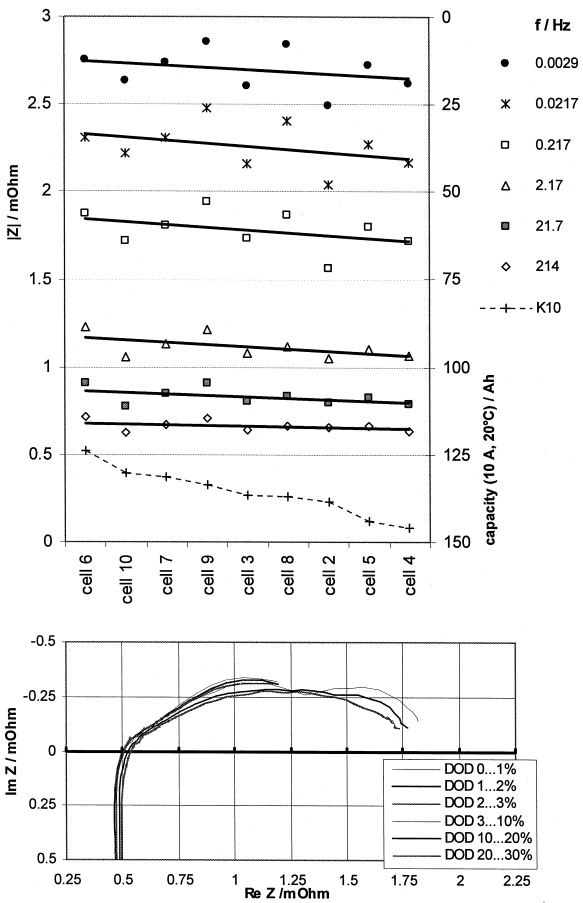

Fig. 8. Impedance and capacity K_{10} (dotted line) of nine cells (no. 2 to 10) at fixed frequencies, measured during continuous discharge between DOD ≅ 20–30%, $I_{dc} = -10$ A, $\vartheta = 20$°C.

Fig. 9. Impedance plots measured during continuous discharge with $I_{dc} = -10$ A for different DODs, $\vartheta = 60$°C at cell no. 7. Minimum frequency: 280 mHz (short curves: DOD = 0–3%) and 2.8 mHz (long curves: DOD = 3–30%).

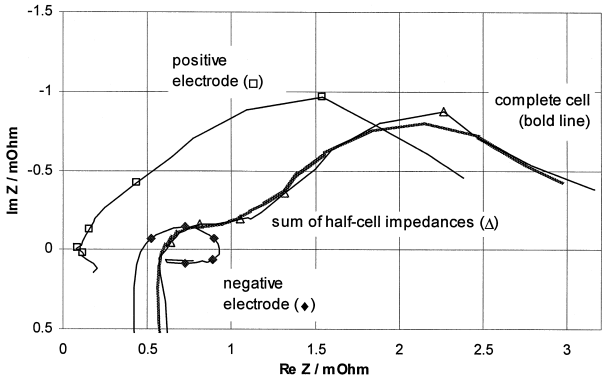

Fig. 10. Impedance plots of half-cells and complete cell at $I_{dc} = -3$ A, DOD ≈ 30%, $\vartheta = 20$°C, measured in discharge/charge mini-cycles at cell no. 16. Minimum frequency: 1.6 mHz. The points corresponding to frequencies $f = 92$ Hz, 9.2 Hz, 920 mHz, 92 mHz, 9.2 mHz are marked.

4.6. Half-cell measurements

Fig. 10 shows the result of half-cell measurements using the mini-cycle technique for DOD starting at 30% and a discharge current of −3 A. The three curves for ''complete cell'' (voltage measured between terminals), ''positive electrode'' (positive terminal vs. reference electrode), and ''negative electrode'' (reference electrode vs. negative terminal) were recorded during subsequent mini-cycles with current always flowing through the terminals, of course. A fourth curve shows simply the result of adding the subsequently measured half-cell impedances which show good coincidence with the ''complete cell'' curve. It can be very clearly seen that the high-frequency part of the cell impedance, above approximately 3 Hz, is almost completely caused by the negative electrode while for frequencies below 3 Hz the positive electrode determines the overall cell behavior. This can offer a possibility to distinguish between the positive vs. negative electrode kinetics without using a reference electrode, simply by measuring in different frequency ranges at the terminals of the cell.

5. Conclusions

The methodology for impedance spectroscopy presented in the first sections of this paper has been applied to a set of 100 Ah lead/acid cells. It showed good reproducibility and consistency of the results. As an alternative to EIS during continuous discharge or charge, a mini-cycle technique was suggested which allows for detailed examination of the battery at fixed SOC. Influence of dc current, SOC, temperature on impedance spectra was determined and discussed. It was also possible to separate the impedances of positive and negative plates from each other both of which dominate the overall cell behavior in different frequency regions. It is shown that impedance spectroscopy can provide detailed information about the processes inside a battery and its state. Depending on the application of a battery, specialized EIS-based measurements will be important diagnostic tools. Future work will be devoted to further extension of the experimental data base for this type of cell, development of a consistent equivalent-circuit model, analysis of SOC and SOH correlation with impedance, and application of the methodology presented here to other battery types.

References

[1] J.R. Macdonald, Impedance Spectroscopy: Emphasizing Solid Materials and Systems, Wiley-Interscience, ISBN 0-471-83122-0, 1987.
[2] F. Huet, J. Power Sources 70 (1998) 59–69.
[3] D.O. Feder, M.J. Hlavac, S.J. McShane, J. Power Sources 48 (1994) 135–161.
[4] Z. Stoynov, Fourier Analysis in the Presence of Nonstationary Aperiodic Noise, Dissertation, ETH Zürich, 1985.
[5] P. Mauracher, E. Karden, J. Power Sources 67 (1997) 69–84.
[6] E. Karden, R.W. De Doncker, Joint International Meeting of the Electrochemical Society and the International Society of Electrochemistry, Paris, 1997.
[7] E. Karden, P. Mauracher, Measurement of the Ultra-low Frequency Impedance of Lead–Acid Batteries, LABAT'96, Varna, Bulgaria, 1996.
[8] M. Keddam, Z. Stoynov, H. Takenouti, J. Appl. Electrochem. 7 (1977) 539–544.